Recurrent Video Restoration Transformer with Guided Deformable Attention

Jingyun Liang[1], **Yuchen Fan**[2], **Xiaoyu Xiang**[2], **Rakesh Ranjan**[2], **Eddy Ilg**[2]
Simon Green[2], **Jiezhang Cao**[1], **Kai Zhang**[1], **Radu Timofte**[1,3], **Luc Van Gool**[1]

[1]Computer Vision Lab, ETH Zurich, Switzerland [2]Meta Inc. [3]University of Wurzburg, Germany

Abstract

Video restoration aims at restoring multiple high-quality frames from multiple low-quality frames. Existing video restoration methods generally fall into two extreme cases, *i.e.*, they either restore all frames in parallel or restore the video frame by frame in a recurrent way, which would result in different merits and drawbacks. Typically, the former has the advantage of temporal information fusion. However, it suffers from large model size and intensive memory consumption; the latter has a relatively small model size as it shares parameters across frames; however, it lacks long-range dependency modeling ability and parallelizability. In this paper, we attempt to integrate the advantages of the two cases by proposing a recurrent video restoration transformer, namely RVRT. RVRT processes local neighboring frames in parallel within a globally recurrent framework which can achieve a good trade-off between model size, effectiveness, and efficiency. Specifically, RVRT divides the video into multiple clips and uses the previously inferred clip feature to estimate the subsequent clip feature. Within each clip, different frame features are jointly updated with implicit feature aggregation. Across different clips, the guided deformable attention is designed for clip-to-clip alignment, which predicts multiple relevant locations from the whole inferred clip and aggregates their features by the attention mechanism. Extensive experiments on video super-resolution, deblurring, and denoising show that the proposed RVRT achieves state-of-the-art performance on benchmark datasets with balanced model size, testing memory and runtime. The codes are available at `https://github.com/JingyunLiang/RVRT`.

1 Introduction

Video restoration, such as video super-resolution, deblurring, and denoising, has become a hot topic in recent years. It aims to restore a clear and sharp high-quality video from a degraded (*e.g.*, downsampled, blurred, or noisy) low-quality video [77, 8, 4, 36]. It has wide applications in live streaming [95], video surveillance [47], old film restoration [75], and more.

Parallel methods and recurrent methods have been dominant strategies for solving various video restoration problems. Typically, those two kinds of methods have their respective merits and demerits. Parallel methods [2, 22, 77, 71, 34, 61, 97, 24, 33, 4, 36] support distributed deployment and achieve good performance by directly fusing information from multiple frames, but they often have a large model size and consume enormous memory for long-sequence videos. In the meanwhile, recurrent models [21, 57, 18, 20, 23, 25, 7, 8, 43, 53, 96, 60] reuse the same network block to save parameters and predict the new frame feature based on the previously refined frame feature, but the sequential processing strategy inevitably leads to information loss and noise amplification [11] for long-range dependency modelling and makes it hard to be parallelized.

Considering the advantages and disadvantages of parallel and recurrent methods, in this paper, we propose a recurrent video restoration transformer (RVRT) that takes **the best of both worlds**. On

Preprint. Under review.

the one hand, RVRT introduces the recurrent design into transformer-based models to reduce model parameters and memory usage. On the other hand, it processes neighboring frames together as a clip to reduce video sequence length and alleviate information loss. To be specific, we first divide the video into fixed-length video clips. Then, starting from the first clip, we refine the subsequent clip feature based on the previously inferred clip feature and the old features of the current clip from shallower layers. Within each clip, different frame features are jointly extracted, implicitly aligned and effectively fused by the self-attention mechanism [74, 49, 37]. Across different clips, information is accumulated clip by clip with a larger hidden state than previous recurrent methods.

To implement the above RVRT model, one big challenge is how to align different video clips when using the previous clip for feature refinement. Most existing alignment techniques [56, 64, 57, 84, 7, 12, 71, 77, 8, 36] are designed for frame-to-frame alignment. One possible way to apply them to clip-to-clip alignment is by introducing an extra feature fusion stage after aligning all frame pairs. Instead, we propose an one-stage **video-to-video alignment** method named guided deformable attention (GDA). More specifically, for a reference location in the target clip, we first estimate the coordinates of multiple relevant locations from different frames in the supporting clip under the guidance of optical flow, and then aggregate features of all locations dynamically by the attention mechanism.

GDA has several advantages over previous alignment methods: 1) Compared with optical flow-based warping that only samples one point from one frame [57, 84, 7], GDA benefits from multiple relevant locations sampled from the video clip. 2) Unlike mutual attention [36], GDA utilizes features from arbitrary locations without suffering from the small receptive field in local attention or the huge computation burden in global attention. Besides, GDA allows direct attention on non-integer locations with bilinear interpolation. 3) In contrast to deformable convolution [12, 98, 71, 77, 8] that uses a fixed weight in feature aggregation, GDA generates dynamic weights to aggregate features from different locations. It also supports arbitrary location numbers and allows for both frame-to-frame and video-to-video alignment without any modification.

Our contributions can be summarized as follows:

- We propose the recurrent video restoration transformer (RVRT) that extracts features of local neighboring frames from one clip in a joint and parallel way, and refines clip features by accumulating information from previous clips and previous layers. By reducing the video sequence length and transmitting information with a larger hidden state, RVRT alleviates information loss and noise amplification in recurrent networks, and also makes it possible to partially parallelize the model.
- We propose the guided deformable attention (GDA) for one-stage video clip-to-clip alignment. It dynamically aggregates information of relevant locations from the supporting clip.
- Extensive experiments on eight benchmark datasets show that the proposed model achieves state-of-the-art performance in three challenging video restoration tasks: video super-resolution, video deblurring, and video denoising, with balanced model size, memory usage and runtime.

2 Related Work

2.1 Video Restoration

Parallel vs. recurrent methods. Most existing video restoration methods can be classified as parallel or recurrent methods according to their parallelizability. Parallel methods estimate all frames simultaneously, as the refinement of one frame feature is not dependent on the update of other frame features. They can be further divided as sliding window-based methods [2, 22, 77, 69, 71, 76, 34, 61, 97, 97, 24, 70, 58, 33] and transformer-based methods [4, 36]. The former kind of methods typically restore merely the center frame from the neighboring frames and are often tested in a sliding window fashion rather than in parallel. These methods generally consist of four stages: feature extraction, feature alignment, feature fusion, and frame reconstruction. Particularly, in the feature alignment stage, they often align all frames towards the center frame, which leads to quadratic complexity with respect to video length and is hard to be extended for long-sequence videos. Instead, the latter kind of method reconstructs all frames at a time based on the transformer architectures. They jointly extract, align, and fuse features for all frames, achieving significant performance improvements against previous methods. However, current transformer-based methods are laid up with a huge model size and large memory consumption. Different from above parallel

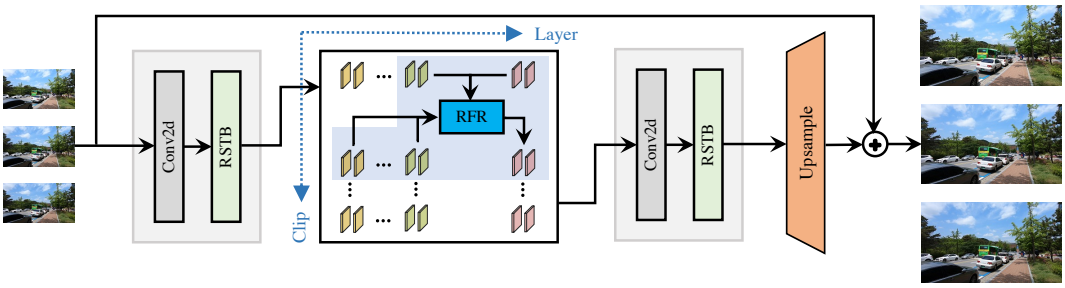

Figure 1: The architecture of recurrent video restoration transformer (RVRT). From left to right, it consists of shallow feature extraction, recurrent feature refinement and HQ frame reconstruction. In recurrent feature refinement (RFR, see more details in Fig. 2), we divide the video into N-frame clips ($N = 2$ in this figure) and process frames in one clip in parallel within a globally recurrent framework in time. Multiple refinement layers are stacked for better performance.

methods, recurrent methods [21, 57, 18, 20, 82, 23, 25, 7, 8, 43, 53, 96, 60] propagate latent features from one frame to the next frame sequentially, where information of previous frames is accumulated for the restoration of later frames. Basically, they are composed of three stages: feature extraction, feature propagation and frame reconstruction. Due to the recurrent nature of feature propagation, recurrent methods suffer from information loss and the inapplicability of distributed deployment.

Alignment in video restoration. Unlike image restoration that mainly focuses on feature extraction [13, 92–94, 40, 38, 39, 66, 91, 90], how to align multiple highly-related but misaligned frames is another key problem in video restoration. Traditionally, many methods [41, 28, 2, 46, 67, 3, 84, 7] first estimate the optical flow between neighbouring frames [16, 56, 64] and then conduct image warping for alignment. Other techniques, such as deformable convolution [12, 98, 71, 77, 8, 4], dynamic filter [27] and mutual attention [36], have also been exploited for implicit feature alignment.

2.2 Vision Transformer

Transformer [74] is the de-facto standard architecture in natural language processing. Recently, it has been used in dealing with vision problems by viewing pixels or image patches as tokens [6, 15], achieving remarkable performance gains in various computer vision tasks, including image classification [15, 35, 49], object detection [73, 48, 81], semantic segmentation [80, 14, 65], *etc*. It also achieves promising results in restoration tasks [10, 37, 78, 42, 4, 36, 17, 19, 5, 87, 45]. In particular, for video restoration, Cao *et al*. [4] propose the first transformer model for video SR, while Liang *et al*. [36] propose an unified framework for video SR, deblurring and denoising.

We note that some transformer-based works [99, 81] have tried to combine the concept of deformation [12, 98] with the attention mechanism [74]. Zhu *et al*. [99] directly predicts the attention weight from the query feature without considering its feature interaction with supporting locations. Concurrently, Xia *et al*. [81] place the supporting points uniformly on the image to make use of global information. Both above two methods are proposed for recognition tasks such as object detection, which is fundamentally different from video alignment in our model.

3 Methodology

3.1 Overall Architecture

Given a low-quality video sequence $I^{LQ} \in \mathbb{R}^{T\times H\times W\times C}$, where T, H, W and C are the video length, height, width and channel, respectively, the goal of video restoration is to reconstruct the high-quality video $I^{HQ} \in \mathbb{R}^{T\times sH\times sW\times C}$, where s is the scale factor. To reach this goal, we propose a recurrent video restoration transformer, as illustrated in Fig. 1. The model consists of three parts: shallow feature extraction, recurrent feature refinement and HQ frame reconstruction. More specifically, in shallow feature extraction, we first use a convolution layer to extract features from the LQ video. For deblurring and denoising (*i.e*., $s = 1$), we additionally add two strided convolution layers to downsample the feature and reduce computation burden in the next layers. After that, several Residual Swin Transformer Blocks (RSTBs) [37] are used to extract the shallow feature. Then, we use recurrent

feature refinement modules for temporal correspondence modeling and guided deformable attention for video alignment, which are detailed in Sec. 3.2 and Sec. 3.3, respectively. Lastly, we add several RSTBs to generate the final feature and reconstruct the HQ video I^{RHQ} by pixel shuffle layer [59]. For training, the Charbonnier loss [9] $\mathcal{L} = \sqrt{\|I^{RHQ} - I^{HQ}\|^2 + \epsilon^2}$ ($\epsilon = 10^{-3}$) is used for all tasks.

3.2 Recurrent Feature Refinement

We stack L recurrent feature refinement modules to refine the video feature by exploiting the temporal correspondence between different frames. To make a trade-off between recurrent and transformer-based methods, we process N frames locally in parallel on the basis of a globally recurrent framework.

Formally, given the video feature $F^i \in \mathbb{R}^{T\times H\times W\times C}$ from the i-th layer, we first reshape it as a 5-dimensional tensor $F^i \in \mathbb{R}^{\frac{T}{N}\times N\times H\times W\times C}$ by dividing it into $\frac{T}{N}$ video clip features: $F^i_1, F^i_2, ..., F^i_{\frac{T}{N}} \in \mathbb{R}^{N\times H\times W\times C}$. Each clip feature F^i_t ($1 \le t \le \frac{T}{N}$) has N neighbouring frame features: $F^i_{t,1}, F^i_{t,2}, ..., F^i_{t,N} \in \mathbb{R}^{H\times W\times C}$. To utilize information from neighbouring clips, we align the $(t-1)$-th clip feature F^i_{t-1} towards the t-th clip based on the optical flow $O^i_{t-1\to t}$, clip feature F^{i-1}_{t-1} and clip feature F^{i-1}_t. This is formulated as follows:

$$\widehat{F}^i_{t-1} = \textit{GDA}(F^i_{t-1}; O^i_{t-1\to t}, F^{i-1}_{t-1}, F^{i-1}_t), \quad (1)$$

where *GDA* is the guided deformable attention and $\widehat{F}^i_{t-1}$ is the aligned clip feature. The details of GDA will be described in Sec. 3.3.

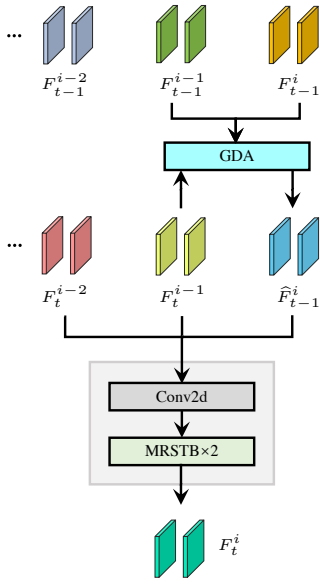

Figure 2: The illustrations of recurrent feature refinement (RFR). The $(t-1)$-th clip feature F^i_{t-1} from the i-th layer is aligned towards the t-th clip as $\widehat{F}^i_{t-1}$ by guided deformable attention (GDA, see more details in Fig. 3). $F^0_t, F^1_t, ..., F^{i-1}_t$ and $\widehat{F}^i_{t-1}$ are then refined as F^i_t by several modified residual swin transformer blocks (MRSTBs), in which different frames are jointly processed in a parallel way.

Similar to recurrent neural networks [57, 7, 8], as shown in Fig. 2, we update the clip feature of each time step as follows:

$$F^i_t = \textit{RFR}(F^0_t, F^1_t, ..., F^{i-1}_t, \widehat{F}^i_{t-1}), \quad (2)$$

where F^0_t is the output of the shallow feature extraction module and $F^1_t, F^2_t, ..., F^{i-1}_t$ are from previous recurrent feature refinement modules. $\textit{RFR}(\cdot)$ is the recurrent feature refinement module that consists of a convolution layer for feature fusion and several modified residual Swin Transformer blocks (*MRSTBs*) for feature refinement. In *MRSTB*, we upgrade the original 2D $h \times w$ attention window to the 3D $N \times h \times w$ attention window, so that every frame in the clip can attend to itself and other frames simultaneously, allowing implicit feature aggregation. In addition, in order to accumulate information forward and backward in time, we reverse the video sequence for all even recurrent feature refinement modules [21, 8].

The above recurrent feature refinement module is the key component of the proposed RVRT model. Globally, features of different video clips are propagated in a recurrent way. Locally, features of different frames are updated jointly in parallel. For an arbitrary single frame, it can make full use of global information accumulated in time and local information extracted together by the self-attention mechanism. As we can see, RVRT is a generalization of both recurrent and transformer models. It becomes a recurrent model when $N = 1$ or a transformer model when $N = T$. This is fundamentally different from previous methods that simply adopt transformer blocks to replace CNN blocks within a recurrent architecture [75]. It is also different from existing attempts in natural language processing [79, 32].

3.3 Guided Deformable Attention for Video Alignment

Different from previous frameworks, the proposed RVRT needs to align neighboring related but misaligned video clips, as indicated in Eq. (1). In this subsection, we propose the guided deformation attention (GDA) for video clip-to-clip alignment.

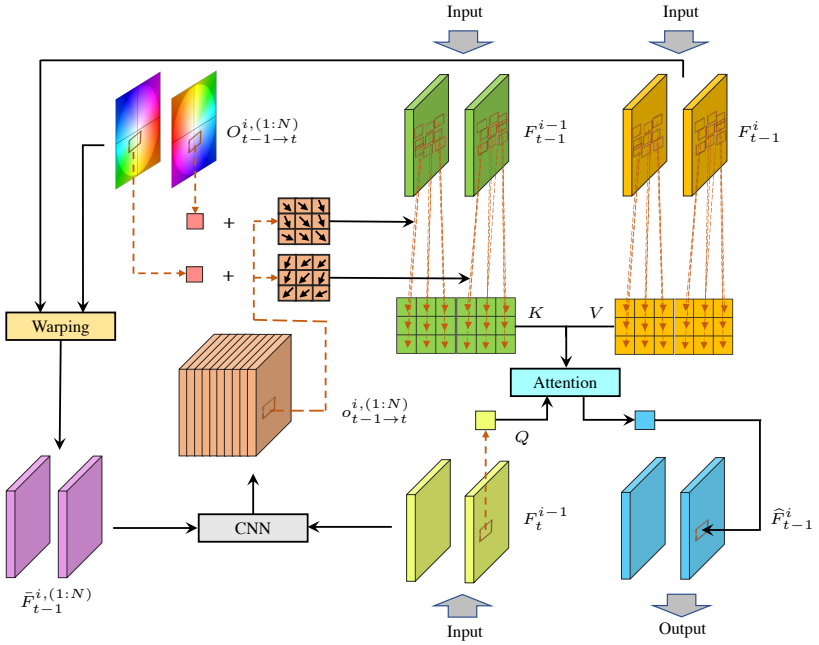

Figure 3: The illustrations of guided deformable attention (GDA). We estimate offsets of multiple relevant locations from different frames based on the warped clip, and then aggregate features of different locations dynamically by the attention mechanism. F^i_{t-1} is the $(t-1)$-th clip feature from the i-th layer, while $\bar{F}^i_{t-1}$ and $\widehat{F}^i_{t-1}$ are the pre-aligned and aligned features of F^i_{t-1}. $O^{i,(1:N)}_{t-1\to t}$ and $o^{i,(1:N)}_{t-1\to t}$ denote optical flows and offsets, respectively.

Given the $(t-1)$-th clip feature F^i_{t-1} from the i-th layer, our goal is to align F^i_{t-1} towards the t-th clip as a list of features $\widehat{F}^{i,(1:N)}_{t-1} = \widehat{F}^{i,(1)}_{t-1}, \widehat{F}^{i,(2)}_{t-1}, ..., \widehat{F}^{i,(N)}_{t-1}$, where $\widehat{F}^{i,(n)}_{t-1} (1 \le n \le N)$ denotes the aligned clip feature towards the n-th frame feature $F^i_{t,n}$ of the t-th clip, and $\widehat{F}^{i,(n)}_{t-1,n'} (1 \le n' \le N)$ is the aligned frame feature from the n'-th frame in the $(t-1)$-th clip to the n-th frame in the t-th clip. Inspired by optical flow estimation designs [16, 54, 64, 8], we first pre-align $F^{i,(n)}_{t-1,n'}$ with the optical flow $O^{i,(n)}_{t-1\to t,n'}$ as $\bar{F}^{i,(n)}_{t-1,n'} = \mathcal{W}(F^{i,(n)}_{t-1,n'}, O^{i,(n)}_{t-1\to t,n'})$, where $\mathcal{W}$ denotes the warping operation. For convenience, we summarize the pre-alignments of all "n'-to-n" $(1 \le n', n \le N)$ frame pairs between the $(t-1)$-th and t-th video clips as follows:

$$\bar{F}^{i,(1:N)}_{t-1} = \mathcal{W}(F^i_{t-1}, O^{i,(1:N)}_{t-1\to t}), \tag{3}$$

After that, we predict the optical flow offsets $o^{i,(1:N)}_{t-1\to t}$ from the concatenation of F^{i-1}_t, $\bar{F}^{i(1:N)}_{t-1}$ and $O^{i,(1:N)}_{t-1\to t}$ along the channel dimension. A small convolutional neural network (CNN) with several convolutional layers and ReLU layers is used for prediction. This is formulated as

$$o^{i,(1:N)}_{t-1\to t} = CNN(Concat(F^{i-1}_t, \bar{F}^{i,(1:N)}_{t-1}, O^{i,(1:N)}_{t-1\to t})), \tag{4}$$

where the current misalignment between the t-th clip feature and the warped $(t-1)$-th clip features can reflect the offset required for further alignment. In practice, we initialize $O^{1,(1:N)}_{t-1\to t}$ as the optical flows estimated from the LQ input video via SpyNet [56], and predict M offsets for each frame (NM offsets in total). The optical flows are updated layer by layer as follows:

$$O^{i+1,(n)}_{t-1\to t,n'} = O^{i,(n)}_{t-1\to t,n'} + \frac{1}{M}\sum_{m=1}^{M}\{o^{i,(n)}_{t-1\to t,n'}\}_m, \tag{5}$$

where $\{o^{i,(n)}_{t-1\to t,n'}\}_m$ denotes the m-th offset in M predictions from the n'-th frame to the n-th frame.

Then, for the n-th frame of the t-th clip, we sample its relevant features from the $(t-1)$-th clip feature F^i_{t-1} according the predicted locations, which are indicated by the sum of optical flow and offsets, *i.e.*,

$O^{i,(n)}_{t-1\to t} + o^{i,(n)}_{t-1\to t}$, according to the chain relationship $F^i_{t-1} \xrightarrow{O^{i,(n)}_{t-1\to t}} \bar{F}^{i,(n)}_{t-1} \xrightarrow{o^{i,(n)}_{t-1\to t}} \widehat{F}^{i,(n)}_{t-1}$ [8, 56]. For simplicity, we define the queries Q, keys K and values V as follows:

$$Q = F^{i-1}_{t,n} P_Q, \tag{6}$$

$$K = \textit{Sampling}(F^{i-1}_{t-1} P_K, O^{i,(n)}_{t-1\to t} + o^{i,(n)}_{t-1\to t}), \tag{7}$$

$$V = \textit{Sampling}(F^{i}_{t-1} P_V, O^{i,(n)}_{t-1\to t} + o^{i,(n)}_{t-1\to t}), \tag{8}$$

where $Q \in \mathbb{R}^{1\times C}$ is the projected feature from the n-th frame of t-th clip. $K \in \mathbb{R}^{NM\times C}$ and $V \in \mathbb{R}^{NM\times C}$ are the projected features that are bilinearly sampled from NM locations of F^{i-1}_{t-1} and F^{i}_{t-1}, respectively. $P_Q \in \mathbb{R}^{C\times C}$, $P_K \in \mathbb{R}^{C\times C}$ and $P_V \in \mathbb{R}^{C\times C}$ are the projection matrices. Note that we first project the feature and then do sampling to reduce redundant computation.

Next, similar to the attention mechanism [74], we calculate the attention weights based on the Q and K from the $(i-1)$-th layer and then compute the aligned feature $\widehat{F}^{i,(n)}_{t-1}$ as a weighted sum of V from the same i-th layer as follows:

$$\widehat{F}^{i,(n)}_{t-1} = \textit{SoftMax}(QK^T/\sqrt{C}))V, \tag{9}$$

where *SoftMax* is the softmax operation along the row direction and $\sqrt{C}$ is a scaling factor.

Lastly, since Eq. (9) only aggregates information spatially, we add a multi-layer perception (*MLP*) with two fully-connected layers and a *GELU* activation function between them to enable channel interaction as follows:

$$\widehat{F}^{i}_{t-1} = \widehat{F}^{i}_{t-1} + \textit{MLP}(\widehat{F}^{i}_{t-1}), \tag{10}$$

where a residual connection is used to stabilize training. The hidden and output channel numbers of the *MLP* are RC (R is the ratio) and C, respectively.

Multi-group multi-head guided deformable attention. We can divide the channel into several deformable groups and perform the deformable sampling for different groups in parallel. Besides, in the attention mechanism, we can further divide one deformable group into several attention heads and perform the attention operation separately for different heads. All groups and heads are concatenated together before channel interaction.

Connection to deformable convolution. Deformable convolution [12, 98] uses a learned weight for feature aggregation, which can be seen as a special case of GDA, *i.e.*, using different projection matrix P_V for different locations and then directly averaging the resulting features. Its parameter number and computation complexity are MC^2 and $\mathcal{O}(MC^2)$, respectively. In contrast, GDA uses the same projection matrix for all locations but generates dynamic weights to aggregate them. Its parameter number and computation complexity are $(3+2R)C^2$ and $\mathcal{O}((3C+2RC+M)C)$, which are similar to deformable convolution when choosing proper M and R.

4 Experiments

4.1 Experimental Setup

For shallow feature extraction and HQ frame reconstruction, we use 1 RSTB that has 2 swin transformer layers. For recurrent feature refinement, we use 4 refinement modules with a clip size of 2, each of which has 2 MRSTBs with 2 modified swin transformer layers. For both RSTB and MRSTB, spatial attention window size and head number are 8×8 and 6, respectively. We use 144 channels for video SR and 192 channels for deblurring and denoising. In GDA, we use 12 deformable groups and 12 deformable heads with 9 candidate locations. We empirically project the query to a higher-dimensional space (*e.g.*, $2C$) because we found it can improve the performance slightly and the parameter number of GDA is not a bottleneck. In training, we randomly crop 256×256 HQ patches and use different video lengths for different datasets: 30 frames for REDS [51], 14 frames for Vimeo-90K [84], and 16 frames for DVD [61], GoPro [52] as well as DAVIS [29]. Adam optimizer [31] with default setting is used to train the model for 600,000 iterations when the batch size is 8. The learning rate is initialized as 4×10^{-4} and deceased with the Cosine Annealing scheme [50]. To stabilize training, we initialize SpyNet [56, 54] with pretrained weights, fix it for the first 30,000 iterations and reduce its learning rate by 75%.

Table 1: Ablation study on clip length.

Clip Length	1	2	3
PSNR	31.98	32.10	32.07

Table 2: Ablation study on different video alignment techniques.

Alignment	None	Warping [84]	TMSA [36]	DCN [71]	GDA*	GDA
PSNR	26.14	28.88	30.45	31.93	32.00	32.10

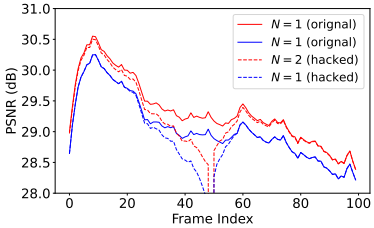

Figure 4: Per-frame PSNR drop when pixels of the 50-th frame is hacked to be all zeros. N is clip length.

Optical Flow Guidance		✓	✓	✓
Optical Flow Update			✓	✓
MLP	✓	✓		✓
PSNR	30.99	32.03	31.83	32.10

Table 3: Ablation study on different GDA components.

Deformable Group	1	6	12	12	12	24
Attention Head	1	6	12	24	36	24
PSNR	31.63	32.03	32.10	32.13	32.03	32.11

Table 4: Ablation study on deformable groups and attention heads.

4.2 Ablation Study

To explore the effectiveness of different components, we conduct ablation studies on REDS [51] for video SR. For efficiency, we reduce the MRSTB blocks by half and use 12 frames in training.

The impact of clip length. In RVRT, we divide the video into N-frame clips. As shown in Table 1, the performance rises when clip length is increased from 1 to 2. However, the performance saturates when $N = 3$, possibly due to the fact that long-range optical flow guidance between distant frames is often inaccurate [26]. Besides, to compare the temporal modelling ability, we hack the input LQ video (Clip 000 from REDS, 100 frames in total) by manually setting all pixels of the 50-th frame as zeros. As indicated in Fig. 4, on the one hand, $N = 2$ has a smaller performance drop and all its frames still have higher PSNR than $N = 1$ (equals to a recurrent model) after the attack, showing that RVRT can mitigate the noise amplification from the hacked frame to the rest frames. One the other hand, the hacked frame of $N = 2$ has an impact on more neighbouring frames than $N = 1$, which means that RVRT can alleviate information loss and utilize more frames than $N = 1$ for restoration.

The impact of video alignment. The alignment of video clips plays a key role in our framework. We compare the proposed clip-to-clip guided deformable attention (GDA) with existing frame-to-frame alignment techniques by performing them frame by frame, followed by concatenation and channel reduction. As we can see from Table 2, GDA outperforms all existing methods when it is used for frame-to-frame alignment (denoted as GDA*), and leads a further improvement when we aggregate features directly from the whole clip.

The impact of different components in GDA. We further conduct an ablation study on GDA in Table 3. As we can see, the optical flow guidance is critical for the model, leading to a PSNR gain of 1.11dB. The update of optical flow in different layers can further improve the result. The channel interaction in MLP also plays an important role, since the attention mechanism only aggregates information spatially.

The impact of deformable group and attention head. We also conduct experiments on different group and head numbers in GDA. As shown in Table 4, when the deformable group rises, the PSNR first rises and then keeps almost unchanged. Besides, double attention heads lead to slightly better results at the expense of higher computation, but using too many heads has an adverse impact as the head dimension may be too small.

4.3 Video Super-Resolution

For video SR, we consider two settings: bicubic (BI) and blur-downsampling (BD) degradation. For BI degradation, we train the model on two different datasets: REDS [51] and Vimeo-90K [84], and then test the model on their corresponding testsets: REDS4 and Vimeo-90K-T. We additionally test Vid4 [44] along with Vimeo-90K. For BD degradation, we train it on Vimeo-90K and test it on Vimeo-90K-T, Vid4, and UDM10 [86]. The comparisons with existing methods are shown in Table 5. As we can see, RVRT achieves the best performance on REDS4 and Vid4 for both degradations. Compared with the representative recurrent model BasicVSR++ [8], RVRT improves the PSNR by significant margins of **0.2**$\sim$**0.5dB**. Compared with the recent transformer-based model VRT [36],

Table 5: Quantitative comparison (average PSNR/SSIM) with state-of-the-art methods for **video super-resolution** ($\times 4$) on **REDS4** [51], **Vimeo-90K-T** [84], **Vid4** [44] and **UDM10** [86].

Method	BI degradation			BD degradation		
	REDS4 [51] (RGB channel)	Vimeo-90K-T [84] (Y channel)	Vid4 [44] (Y channel)	UDM10 [86] (Y channel)	Vimeo-90K-T [84] (Y channel)	Vid4 [44] (Y channel)
Bicubic	26.14/0.7292	31.32/0.8684	23.78/0.6347	28.47/0.8253	31.30/0.8687	21.80/0.5246
SwinIR [37]	29.05/0.8269	35.67/0.9287	25.68/0.7491	35.42/0.9380	34.12/0.9167	25.25/0.7262
SwinIR-ft [37]	29.24/0.8319	35.89/0.9301	25.69/0.7488	36.76/0.9467	35.70/0.9293	25.62/0.7498
TOFlow [84]	27.98/0.7990	33.08/0.9054	25.89/0.7651	36.26/0.9438	34.62/0.9212	25.85/0.7659
FRVSR [57]	-	-	-	37.09/0.9522	35.64/0.9319	26.69/0.8103
DUF [27]	28.63/0.8251	-	27.33/0.8319	38.48/0.9605	36.87/0.9447	27.38/0.8329
PFNL [86]	29.63/0.8502	36.14/0.9363	26.73/0.8029	38.74/0.9627	-	27.16/0.8355
RBPN [20]	30.09/0.8590	37.07/0.9435	27.12/0.8180	38.66/0.9596	37.20/0.9458	27.17/0.8205
MuCAN [34]	30.88/0.8750	37.32/0.9465	-	-	-	-
RLSP [18]	-	-	-	38.48/0.9606	36.49/0.9403	27.48/0.8388
TGA [24]	-	-	-	38.74/0.9627	37.59/0.9516	27.63/0.8423
RSDN [23]	-	-	-	39.35/0.9653	37.23/0.9471	27.92/0.8505
RRN [25]	-	-	-	38.96/0.9644	-	27.69/0.8488
FDAN [43]	-	-	-	39.91/0.9686	37.75/0.9522	27.88/0.8508
EDVR [77]	31.09/0.8800	37.61/0.9489	27.35/0.8264	39.89/0.9686	37.81/0.9523	27.85/0.8503
GOVSR [85]	-	-	-	40.14/0.9713	37.63/0.9503	28.41/0.8724
BasicVSR [7]	31.42/0.8909	37.18/0.9450	27.24/0.8251	39.96/0.9694	37.53/0.9498	27.96/0.8553
IconVSR [7]	31.67/0.8948	37.47/0.9476	27.39/0.8279	40.03/0.9694	37.84/0.9524	28.04/0.8570
VRT [36]	32.19/0.9006	38.20/0.9530	27.93/0.8425	41.05/0.9737	38.72/0.9584	29.42/0.8795
BasicVSR++ [8]	32.39/0.9069	37.79/0.9500	27.79/0.8400	40.72/0.9722	38.21/0.9550	29.04/0.8753
RVRT (ours)	32.75/0.9113	38.15/0.9527	27.99/0.8462	40.90/0.9729	38.59/0.9576	29.54/0.8810

Table 6: Comparison of model size, testing memory and runtime for an LQ input of 320×180.

Method	#Param (M)	Memory (M)	Runtime (ms)	PSNR (dB)
BasicVSR++ [8]	7.3	223	77	32.39
BasicVSR++ [8]+RSTB [37]	9.3	1021	201	32.61
EDVR [77]	20.6	3535	378	31.09
VSRT [4]	32.6	27487	328	31.19
VRT [36]	35.6	2149	243	32.19
RVRT (ours)	10.8	1056	183	32.75

RVRT outperforms VRT on REDS4 and Vid4 by **up to 0.36dB**. The visual comparisons of different methods are shown in Fig. 5. It is clear that RVRT generates sharp and clear HQ frames, while other methods fail to restore fine textures and details.

We compare the model size, testing memory consumption and runtime of different models in Table 6. Compared with representative parallel methods EDVR [77], VSRT [4] and VST [36], RVRT achieves significant performance gains with less than **at least 50%** of model parameters and testing memory usage. It also reduces the runtime by **at least 25%**. Compared the recurrent model BasicVSR++ [8], RVRT brings a PSNR improvement of 0.26dB. As for the inferiority of testing memory and runtime, we argue that it is mainly because the CNN layers are highly optimized on existing deep learning frameworks. To prove it, we use the transformer-based RSTB blocks in RVRT to replace the CNN blocks in BasicVSR++, in which case it has similar memory usage and more runtime than our model.

In addition, to better understand how guided deformable attention works, we visualize the predicted offsets on the LQ frames and show the attention weight in Fig. 6. As we can see, multiple offsets are predicted to select multiple sampled locations in the neighbourhood of the corresponding pixel. According to the feature similarity between the query feature and the sampled features, features of different locations are aggregated by calculating a dynamic attention weight.

4.4 Video Deblurring

For video deblurring, the model is trained and tested on two different datasets, DVD [61] and GoPro [52], with their official training/testing splits. As shown in Table 7 and 8, RVRT shows its superiority over most methods with huge improvements of **1.40$\sim$2.27dB** on two datasets. Even though the performance gain over VRT is relatively small, RVRT has a smaller model size and much less runtime. In detail, the model size and runtime of RVRT are 13.6M and 0.3s, while VRT has 18.3M parameters and the runtime of 2.2s on a 1280×720 LQ input. The visual comparison is provided in the supplementary material due to the space limit.

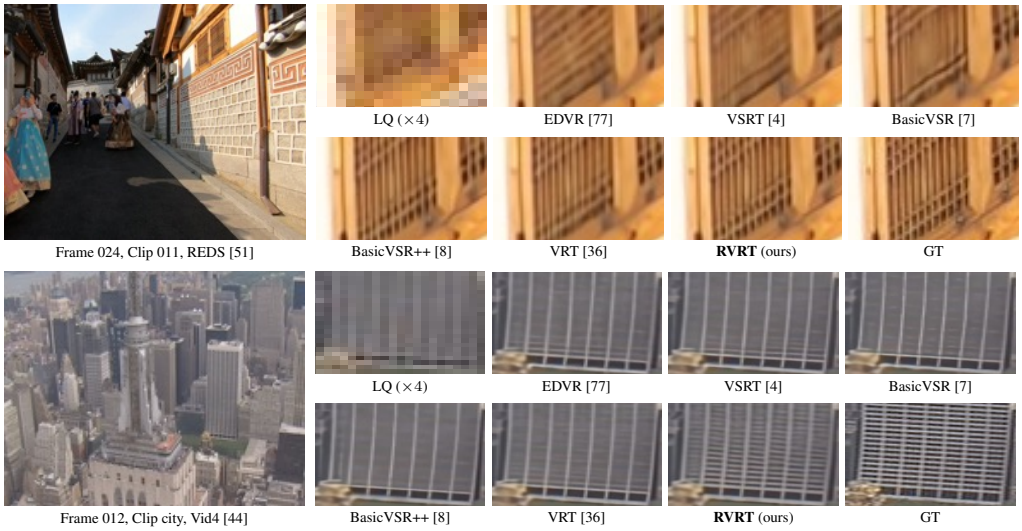

Figure 5: Visual comparison of **video super-resolution** ($\times 4$) methods on REDS [51] and Vid4 [44].

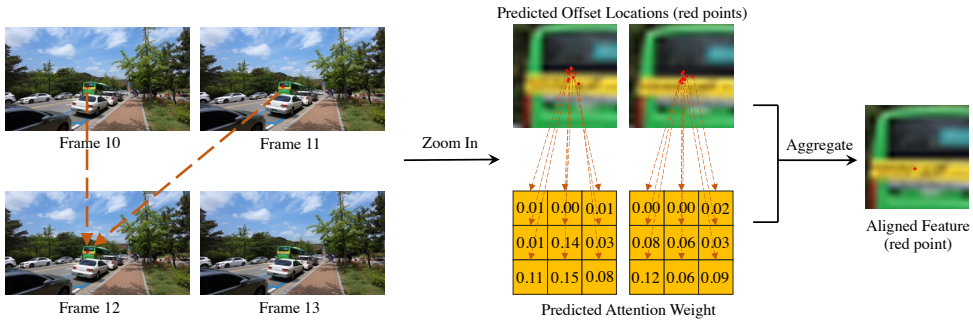

Figure 6: The visualization of predicted offsets and attention weight predicted in guided deformable attention. Although guided deformable attention is conducted on features, we plot illustrations on LQ input frames for better understanding. Best viewed by zooming.

4.5 Video Denoising

For video denoising, we train the model on the training set of DAVIS [29] and test it on its corresponding testset and Set8 [69]. For fairness of comparison, following [69, 70], we train a non-blind additive white Gaussian denoising model for noise level $\sigma \sim \mathcal{U}(0, 50)$. Similar to the case of video deblurring, there is a huge gap (**0.60∼2.37dB**) between RVRT and most methods. Compared with VRT, RVRT has slightly better performance on large noise levels, with a smaller model size (12.8M *v.s.*18.4M) and less runtime (0.2s *v.s.*1.5s) on a 1280×720 LQ input. The visual comparison is provided in the supplementary material due to the space limit.

5 Conclusion

In this paper, we proposed a recurrent video restoration transformer with guided deformable attention. It is a globally recurrent model with locally parallel designs, which benefits from the advantages of both parallel methods and recurrent methods. We also propose the guided deformable attention module for our special case of video clip-to-clip alignment. Under the guidance of optical flow, it aggregates information from multiple neighboring locations adaptively with the attention mechanism. Extensive experiments on video super-resolution, video deblurring, and video denoising demonstrated the effectiveness of the proposed method.

Table 7: Quantitative comparison (average RGB channel PSNR/SSIM) with state-of-the-art methods for **video deblurring** on **DVD** [61].

Method	SRN [68]	DBN [61]	STFAN [97]	STTN [30]	SFE [83]	EDVR [77]
PSNR	30.53	30.01	31.24	31.61	31.71	31.82
SSIM	0.8940	0.8877	0.9340	0.9160	0.9160	0.9160
Method	TSP [55]	PVDNet [60]	GSTA [63]	ARVo [33]	VRT [36]	**RVRT** (ours)
PSNR	32.13	32.31	32.53	32.80	34.24	34.30
SSIM	0.9268	0.9260	0.9468	0.9352	0.9651	0.9655

Table 8: Quantitative comparison (average RGB channel PSNR/SSIM) with state-of-the-art methods for **video deblurring** on **GoPro** [52].

Method	SRN [68]	DMPHN [89]	SAPHN [62]	MPRNet [88]	IFI-RNN [53]	ESTRNN [96]
PSNR	30.26	31.20	31.85	32.66	31.05	31.07
SSIM	0.9342	0.9400	0.9480	0.9590	0.9110	0.9023
Method	EDVR [77]	TSP [55]	PVDNet [60]	GSTA [63]	VRT [36]	**RVRT** (ours)
PSNR	31.54	31.67	31.98	32.10	34.81	34.92
SSIM	0.9260	0.9279	0.9280	0.9600	0.9724	0.9738

Table 9: Quantitative comparison (average RGB channel PSNR) with state-of-the-art methods for **video denoising** on **DAVIS** [29] and **Set8** [69].

Dataset	σ	VLNB [1]	DVDNet [69]	FastDVDNet [70]	PaCNet [72]	VRT [36]	**RVRT** (ours)
DAVIS	10	38.85	38.13	38.71	39.97	40.82	40.57
	20	35.68	35.70	35.77	36.82	38.15	38.05
	30	33.73	34.08	34.04	34.79	36.52	36.57
	40	32.32	32.86	32.82	33.34	35.32	35.47
	50	31.13	31.85	31.86	32.20	34.36	34.57
Set8	10	37.26	36.08	36.44	37.06	37.88	37.53
	20	33.72	33.49	33.43	33.94	35.02	34.83
	30	31.74	31.79	31.68	32.05	33.35	33.30
	40	30.39	30.55	30.46	30.70	32.15	32.21
	50	29.24	29.56	29.53	29.66	31.22	31.33

6 Limitations and Societal Impacts

Although RVRT achieves state-of-the-art performance in video restoration, it still has some limitations. For example, the complexity of pre-alignment by optical flow increases quadratically with respect to the clip length. One possible solution is to develop a video-to-video optical flow estimation model that directly predicts all optical flows. As for societal impacts, similar to other restoration methods, RVRT may bring privacy concerns after restoring blurry videos and lead to misjudgments if used for medical diagnosis.

Acknowledgments and Disclosure of Funding

This work was partially supported by the ETH Zurich Fund (OK), a Huawei Technologies Oy (Finland) project, the China Scholarship Council and an Amazon AWS grant. Special thanks goes to Yijue Chen.

References

[1] Pablo Arias and Jean-Michel Morel. Video denoising via empirical bayesian estimation of space-time patches. *Journal of Mathematical Imaging and Vision*, 60(1):70–93, 2018.

[2] Jose Caballero, Christian Ledig, Andrew Aitken, Alejandro Acosta, Johannes Totz, Zehan Wang, and Wenzhe Shi. Real-time video super-resolution with spatio-temporal networks and motion compensation. In *IEEE Conference on Computer Vision and Pattern Recognition*, pages 4778–4787, 2017.

[3] Jose Caballero, Christian Ledig, Andrew Aitken, Alejandro Acosta, Johannes Totz, Zehan Wang, and Wenzhe Shi. Real-time video super-resolution with spatio-temporal networks and motion compensation. In *IEEE Conference on Computer Vision and Pattern Recognition*, pages 4778–4787, 2017.

[4] Jiezhang Cao, Yawei Li, Kai Zhang, and Luc Van Gool. Video super-resolution transformer. *arXiv preprint arXiv:2106.06847*, 2021.

[5] Mingdeng Cao, Yanbo Fan, Yong Zhang, Jue Wang, and Yujiu Yang. Vdtr: Video deblurring with transformer. *arXiv preprint arXiv:2204.08023*, 2022.

[6] Nicolas Carion, Francisco Massa, Gabriel Synnaeve, Nicolas Usunier, Alexander Kirillov, and Sergey Zagoruyko. End-to-end object detection with transformers. In *European Conference on Computer Vision*, pages 213–229, 2020.

[7] Kelvin CK Chan, Xintao Wang, Ke Yu, Chao Dong, and Chen Change Loy. Basicvsr: The search for essential components in video super-resolution and beyond. In *IEEE Conference on Computer Vision and Pattern Recognition*, pages 4947–4956, 2021.

[8] Kelvin CK Chan, Shangchen Zhou, Xiangyu Xu, and Chen Change Loy. Basicvsr++: Improving video super-resolution with enhanced propagation and alignment. *arXiv preprint arXiv:2104.13371*, 2021.

[9] Pierre Charbonnier, Laure Blanc-Feraud, Gilles Aubert, and Michel Barlaud. Two deterministic half-quadratic regularization algorithms for computed imaging. In *International Conference on Image Processing*, pages 168–172, 1994.

[10] Hanting Chen, Yunhe Wang, Tianyu Guo, Chang Xu, Yiping Deng, Zhenhua Liu, Siwei Ma, Chunjing Xu, Chao Xu, and Wen Gao. Pre-trained image processing transformer. In *IEEE Conference on Computer Vision and Pattern Recognition*, pages 12299–12310, 2021.

[11] Mengyu Chu, You Xie, Jonas Mayer, Laura Leal-Taixé, and Nils Thuerey. Learning temporal coherence via self-supervision for gan-based video generation. *ACM Transactions on Graphics (TOG)*, 39(4):75–1, 2020.

[12] Jifeng Dai, Haozhi Qi, Yuwen Xiong, Yi Li, Guodong Zhang, Han Hu, and Yichen Wei. Deformable convolutional networks. In *IEEE International Conference on Computer Vision*, pages 764–773, 2017.

[13] Chao Dong, Chen Change Loy, Kaiming He, and Xiaoou Tang. Learning a deep convolutional network for image super-resolution. In *European Conference on Computer Vision*, pages 184–199, 2014.

[14] Xiaoyi Dong, Jianmin Bao, Dongdong Chen, Weiming Zhang, Nenghai Yu, Lu Yuan, Dong Chen, and Baining Guo. Cswin transformer: A general vision transformer backbone with cross-shaped windows. *arXiv preprint arXiv:2107.00652*, 2021.

[15] Alexey Dosovitskiy, Lucas Beyer, Alexander Kolesnikov, Dirk Weissenborn, Xiaohua Zhai, Thomas Unterthiner, Mostafa Dehghani, Matthias Minderer, Georg Heigold, Sylvain Gelly, et al. An image is worth 16x16 words: Transformers for image recognition at scale. *arXiv preprint arXiv:2010.11929*, 2020.

[16] Alexey Dosovitskiy, Philipp Fischer, Eddy Ilg, Philip Hausser, Caner Hazirbas, Vladimir Golkov, Patrick Van Der Smagt, Daniel Cremers, and Thomas Brox. Flownet: Learning optical flow with convolutional networks. In *IEEE International Conference on Computer Vision*, pages 2758–2766, 2015.

[17] Dario Fuoli, Martin Danelljan, Radu Timofte, and Luc Van Gool. Fast online video super-resolution with deformable attention pyramid. *arXiv preprint arXiv:2202.01731*, 2022.

[18] Dario Fuoli, Shuhang Gu, and Radu Timofte. Efficient video super-resolution through recurrent latent space propagation. In *IEEE International Conference on Computer Vision Workshop*, pages 3476–3485, 2019.

[19] Zhicheng Geng, Luming Liang, Tianyu Ding, and Ilya Zharkov. Rstt: Real-time spatial temporal transformer for space-time video super-resolution. *arXiv preprint arXiv:2203.14186*, 2022.

[20] Muhammad Haris, Gregory Shakhnarovich, and Norimichi Ukita. Recurrent back-projection network for video super-resolution. In *IEEE Conference on Computer Vision and Pattern Recognition*, pages 3897–3906, 2019.

[21] Yan Huang, Wei Wang, and Liang Wang. Bidirectional recurrent convolutional networks for multi-frame super-resolution. *Advances in Neural Information Processing Systems*, 28:235–243, 2015.

[22] Yan Huang, Wei Wang, and Liang Wang. Video super-resolution via bidirectional recurrent convolutional networks. *IEEE Transactions on Pattern Analysis and Machine Intelligence*, 40(4):1015–1028, 2017.

[23] Takashi Isobe, Xu Jia, Shuhang Gu, Songjiang Li, Shengjin Wang, and Qi Tian. Video super-resolution with recurrent structure-detail network. In *European Conference on Computer Vision*, pages 645–660, 2020.

[24] Takashi Isobe, Songjiang Li, Xu Jia, Shanxin Yuan, Gregory Slabaugh, Chunjing Xu, Ya-Li Li, Shengjin Wang, and Qi Tian. Video super-resolution with temporal group attention. In *IEEE Conference on Computer Vision and Pattern Recognition*, pages 8008–8017, 2020.

[25] Takashi Isobe, Fang Zhu, Xu Jia, and Shengjin Wang. Revisiting temporal modeling for video super-resolution. *arXiv preprint arXiv:2008.05765*, 2020.

[26] Allan Jabri, Andrew Owens, and Alexei Efros. Space-time correspondence as a contrastive random walk. *Advances in neural information processing systems*, 33:19545–19560, 2020.
[27] Younghyun Jo, Seoung Wug Oh, Jaeyeon Kang, and Seon Joo Kim. Deep video super-resolution network using dynamic upsampling filters without explicit motion compensation. In *IEEE Conference on Computer Vision and Pattern Recognition*, pages 3224–3232, 2018.
[28] Armin Kappeler, Seunghwan Yoo, Qiqin Dai, and Aggelos K Katsaggelos. Video super-resolution with convolutional neural networks. *IEEE Transactions on Computational Imaging*, 2(2):109–122, 2016.
[29] Anna Khoreva, Anna Rohrbach, and Bernt Schiele. Video object segmentation with language referring expressions. In *Asian Conference on Computer Vision*, pages 123–141, 2018.
[30] Tae Hyun Kim, Mehdi SM Sajjadi, Michael Hirsch, and Bernhard Scholkopf. Spatio-temporal transformer network for video restoration. In *European Conference on Computer Vision*, pages 106–122, 2018.
[31] Diederik P Kingma and Jimmy Ba. Adam: A method for stochastic optimization. *arXiv preprint arXiv:1412.6980*, 2014.
[32] Jie Lei, Liwei Wang, Yelong Shen, Dong Yu, Tamara L Berg, and Mohit Bansal. Mart: Memory-augmented recurrent transformer for coherent video paragraph captioning. *arXiv preprint arXiv:2005.05402*, 2020.
[33] Dongxu Li, Chenchen Xu, Kaihao Zhang, Xin Yu, Yiran Zhong, Wenqi Ren, Hanna Suominen, and Hongdong Li. Arvo: Learning all-range volumetric correspondence for video deblurring. In *IEEE Conference on Computer Vision and Pattern Recognition*, pages 7721–7731, 2021.
[34] Wenbo Li, Xin Tao, Taian Guo, Lu Qi, Jiangbo Lu, and Jiaya Jia. Mucan: Multi-correspondence aggregation network for video super-resolution. In *European Conference on Computer Vision*, pages 335–351, 2020.
[35] Yawei Li, Kai Zhang, Jiezhang Cao, Radu Timofte, and Luc Van Gool. Localvit: Bringing locality to vision transformers. *arXiv preprint arXiv:2104.05707*, 2021.
[36] Jingyun Liang, Jiezhang Cao, Yuchen Fan, Kai Zhang, Rakesh Ranjan, Yawei Li, Radu Timofte, and Luc Van Gool. Vrt: A video restoration transformer. *arXiv preprint arXiv:2201.12288*, 2022.
[37] Jingyun Liang, Jiezhang Cao, Guolei Sun, Kai Zhang, Luc Van Gool, and Radu Timofte. SwinIR: Image restoration using swin transformer. In *IEEE Conference on International Conference on Computer Vision Workshops*, 2021.
[38] Jingyun Liang, Andreas Lugmayr, Kai Zhang, Martin Danelljan, Luc Van Gool, and Radu Timofte. Hierarchical conditional flow: A unified framework for image super-resolution and image rescaling. In *IEEE Conference on International Conference on Computer Vision*, 2021.
[39] Jingyun Liang, Guolei Sun, Kai Zhang, Luc Van Gool, and Radu Timofte. Mutual affine network for spatially variant kernel estimation in blind image super-resolution. In *IEEE Conference on International Conference on Computer Vision*, 2021.
[40] Jingyun Liang, Kai Zhang, Shuhang Gu, Luc Van Gool, and Radu Timofte. Flow-based kernel prior with application to blind super-resolution. In *IEEE Conference on Computer Vision and Pattern Recognition*, pages 10601–10610, 2021.
[41] Renjie Liao, Xin Tao, Ruiyu Li, Ziyang Ma, and Jiaya Jia. Video super-resolution via deep draft-ensemble learning. In *IEEE International Conference on Computer Vision*, pages 531–539, 2015.
[42] Jing Lin, Yuanhao Cai, Xiaowan Hu, Haoqian Wang, Youliang Yan, Xueyi Zou, Henghui Ding, Yulun Zhang, Radu Timofte, and Luc Van Gool. Flow-guided sparse transformer for video deblurring. *arXiv preprint arXiv:2201.01893*, 2022.
[43] Jiayi Lin, Yan Huang, and Liang Wang. Fdan: Flow-guided deformable alignment network for video super-resolution. *arXiv preprint arXiv:2105.05640*, 2021.
[44] Ce Liu and Deqing Sun. On bayesian adaptive video super resolution. *IEEE Transactions on Pattern Analysis and Machine Intelligence*, 36(2):346–360, 2013.
[45] Chengxu Liu, Huan Yang, Jianlong Fu, and Xueming Qian. Learning trajectory-aware transformer for video super-resolution. *arXiv preprint arXiv:2204.04216*, 2022.
[46] Ding Liu, Zhaowen Wang, Yuchen Fan, Xianming Liu, Zhangyang Wang, Shiyu Chang, and Thomas Huang. Robust video super-resolution with learned temporal dynamics. In *IEEE International Conference on Computer Vision*, pages 2507–2515, 2017.
[47] Hongying Liu, Zhubo Ruan, Peng Zhao, Chao Dong, Fanhua Shang, Yuanyuan Liu, Linlin Yang, and Radu Timofte. Video super-resolution based on deep learning: a comprehensive survey. *Artificial Intelligence Review*, pages 1–55, 2022.
[48] Li Liu, Wanli Ouyang, Xiaogang Wang, Paul Fieguth, Jie Chen, Xinwang Liu, and Matti Pietikäinen. Deep learning for generic object detection: A survey. *International Journal of*

Computer Vision, 128(2):261–318, 2020.

[49] Ze Liu, Yutong Lin, Yue Cao, Han Hu, Yixuan Wei, Zheng Zhang, Stephen Lin, and Baining Guo. Swin transformer: Hierarchical vision transformer using shifted windows. *arXiv preprint arXiv:2103.14030*, 2021.

[50] Ilya Loshchilov and Frank Hutter. Sgdr: Stochastic gradient descent with warm restarts. *arXiv preprint arXiv:1608.03983*, 2016.

[51] Seungjun Nah, Sungyong Baik, Seokil Hong, Gyeongsik Moon, Sanghyun Son, Radu Timofte, and Kyoung Mu Lee. Ntire 2019 challenge on video deblurring and super-resolution: Dataset and study. In *IEEE Conference on Computer Vision and Pattern Recognition Workshops*, pages 1996–2005, 2019.

[52] Seungjun Nah, Tae Hyun Kim, and Kyoung Mu Lee. Deep multi-scale convolutional neural network for dynamic scene deblurring. In *IEEE Conference on Computer Vision and Pattern Recognition*, pages 3883–3891, 2017.

[53] Seungjun Nah, Sanghyun Son, and Kyoung Mu Lee. Recurrent neural networks with intra-frame iterations for video deblurring. In *IEEE Conference on Computer Vision and Pattern Recognition*, pages 8102–8111, 2019.

[54] Simon Niklaus. A reimplementation of SPyNet using PyTorch. `https://github.com/sniklaus/pytorch-spynet`, 2018.

[55] Jinshan Pan, Haoran Bai, and Jinhui Tang. Cascaded deep video deblurring using temporal sharpness prior. In *IEEE Conference on Computer Vision and Pattern Recognition*, pages 3043–3051, 2020.

[56] Anurag Ranjan and Michael J Black. Optical flow estimation using a spatial pyramid network. In *IEEE Conference on Computer Vision and Pattern Recognition*, pages 4161–4170, 2017.

[57] Mehdi SM Sajjadi, Raviteja Vemulapalli, and Matthew Brown. Frame-recurrent video super-resolution. In *IEEE Conference on Computer Vision and Pattern Recognition*, pages 6626–6634, 2018.

[58] Dev Yashpal Sheth, Sreyas Mohan, Joshua L Vincent, Ramon Manzorro, Peter A Crozier, Mitesh M Khapra, Eero P Simoncelli, and Carlos Fernandez-Granda. Unsupervised deep video denoising. In *IEEE International Conference on Computer Vision*, pages 1759–1768, 2021.

[59] Wenzhe Shi, Jose Caballero, Ferenc Huszár, Johannes Totz, Andrew P Aitken, Rob Bishop, Daniel Rueckert, and Zehan Wang. Real-time single image and video super-resolution using an efficient sub-pixel convolutional neural network. In *IEEE Conference on Computer Vision and Pattern Recognition*, pages 1874–1883, 2016.

[60] Hyeongseok Son, Junyong Lee, Jonghyeop Lee, Sunghyun Cho, and Seungyong Lee. Recurrent video deblurring with blur-invariant motion estimation and pixel volumes. *ACM Transactions on Graphics*, 40(5):1–18, 2021.

[61] Shuochen Su, Mauricio Delbracio, Jue Wang, Guillermo Sapiro, Wolfgang Heidrich, and Oliver Wang. Deep video deblurring for hand-held cameras. In *IEEE Conference on Computer Vision and Pattern Recognition*, pages 1279–1288, 2017.

[62] Maitreya Suin, Kuldeep Purohit, and AN Rajagopalan. Spatially-attentive patch-hierarchical network for adaptive motion deblurring. In *IEEE Conference on Computer Vision and Pattern Recognition*, pages 3606–3615, 2020.

[63] Maitreya Suin and AN Rajagopalan. Gated spatio-temporal attention-guided video deblurring. In *IEEE Conference on Computer Vision and Pattern Recognition*, pages 7802–7811, 2021.

[64] Deqing Sun, Xiaodong Yang, Ming-Yu Liu, and Jan Kautz. Pwc-net: Cnns for optical flow using pyramid, warping, and cost volume. In *IEEE Conference on Computer Vision and Pattern Recognition*, pages 8934–8943, 2018.

[65] Guolei Sun, Yun Liu, Thomas Probst, Danda Pani Paudel, Nikola Popovic, and Luc Van Gool. Boosting crowd counting with transformers. *arXiv preprint arXiv:2105.10926*, 2021.

[66] Lei Sun, Christos Sakaridis, Jingyun Liang, Qi Jiang, Kailun Yang, Peng Sun, Yaozu Ye, Kaiwei Wang, and Luc Van Gool. Mefnet: Multi-scale event fusion network for motion deblurring. *arXiv preprint arXiv:2112.00167*, 2021.

[67] Xin Tao, Hongyun Gao, Renjie Liao, Jue Wang, and Jiaya Jia. Detail-revealing deep video super-resolution. In *IEEE International Conference on Computer Vision*, pages 4472–4480, 2017.

[68] Xin Tao, Hongyun Gao, Xiaoyong Shen, Jue Wang, and Jiaya Jia. Scale-recurrent network for deep image deblurring. In *IEEE Conference on Computer Vision and Pattern Recognition*, pages 8174–8182, 2018.

[69] Matias Tassano, Julie Delon, and Thomas Veit. Dvdnet: A fast network for deep video denoising. In *IEEE International Conference on Image Processing*, pages 1805–1809, 2019.

[70] Matias Tassano, Julie Delon, and Thomas Veit. Fastdvdnet: Towards real-time deep video denoising without flow estimation. In *IEEE Conference on Computer Vision and Pattern Recognition*, pages 1354–1363, 2020.

[71] Yapeng Tian, Yulun Zhang, Yun Fu, and Chenliang Xu. Tdan: Temporally-deformable alignment network for video super-resolution. In *IEEE Conference on Computer Vision and Pattern Recognition*, pages 3360–3369, 2020.

[72] Gregory Vaksman, Michael Elad, and Peyman Milanfar. Patch craft: Video denoising by deep modeling and patch matching. In *IEEE International Conference on Computer Vision*, pages 1759–1768, 2021.

[73] Ashish Vaswani, Prajit Ramachandran, Aravind Srinivas, Niki Parmar, Blake Hechtman, and Jonathon Shlens. Scaling local self-attention for parameter efficient visual backbones. *arXiv preprint arXiv:2103.12731*, 2021.

[74] Ashish Vaswani, Noam Shazeer, Niki Parmar, Jakob Uszkoreit, Llion Jones, Aidan N Gomez, Lukasz Kaiser, and Illia Polosukhin. Attention is all you need. *arXiv preprint arXiv:1706.03762*, 2017.

[75] Ziyu Wan, Bo Zhang, Dongdong Chen, and Jing Liao. Bringing old films back to life. *arXiv preprint arXiv:2203.17276*, 2022.

[76] Longguang Wang, Yulan Guo, Li Liu, Zaiping Lin, Xinpu Deng, and Wei An. Deep video super-resolution using hr optical flow estimation. *IEEE Transactions on Image Processing*, 29:4323–4336, 2020.

[77] Xintao Wang, Kelvin CK Chan, Ke Yu, Chao Dong, and Chen Change Loy. Edvr: Video restoration with enhanced deformable convolutional networks. In *IEEE Conference on Computer Vision and Pattern Recognition Workshops*, pages 1954–1963, 2019.

[78] Zhendong Wang, Xiaodong Cun, Jianmin Bao, and Jianzhuang Liu. Uformer: A general u-shaped transformer for image restoration. *arXiv preprint arXiv:2106.03106*, 2021.

[79] Zhiwei Wang, Yao Ma, Zitao Liu, and Jiliang Tang. R-transformer: Recurrent neural network enhanced transformer. *arXiv preprint arXiv:1907.05572*, 2019.

[80] Bichen Wu, Chenfeng Xu, Xiaoliang Dai, Alvin Wan, Peizhao Zhang, Zhicheng Yan, Masayoshi Tomizuka, Joseph Gonzalez, Kurt Keutzer, and Peter Vajda. Visual transformers: Token-based image representation and processing for computer vision. *arXiv preprint arXiv:2006.03677*, 2020.

[81] Zhuofan Xia, Xuran Pan, Shiji Song, Li Erran Li, and Gao Huang. Vision transformer with deformable attention. *arXiv preprint arXiv:2201.00520*, 2022.

[82] Xiaoyu Xiang, Yapeng Tian, Yulun Zhang, Yun Fu, Jan P Allebach, and Chenliang Xu. Zooming slow-mo: Fast and accurate one-stage space-time video super-resolution. In *IEEE Conference on Computer Vision and Pattern Recognition*, pages 3370–3379, 2020.

[83] Xinguang Xiang, Hao Wei, and Jinshan Pan. Deep video deblurring using sharpness features from exemplars. *IEEE Transactions on Image Processing*, 29:8976–8987, 2020.

[84] Tianfan Xue, Baian Chen, Jiajun Wu, Donglai Wei, and William T Freeman. Video enhancement with task-oriented flow. *International Journal of Computer Vision*, 127(8):1106–1125, 2019.

[85] Peng Yi, Zhongyuan Wang, Kui Jiang, Junjun Jiang, Tao Lu, Xin Tian, and Jiayi Ma. Omniscient video super-resolution. In *IEEE International Conference on Computer Vision*, pages 4429–4438, 2021.

[86] Peng Yi, Zhongyuan Wang, Kui Jiang, Junjun Jiang, and Jiayi Ma. Progressive fusion video super-resolution network via exploiting non-local spatio-temporal correlations. In *IEEE International Conference on Computer Vision*, pages 3106–3115, 2019.

[87] Wulian Yun, Mengshi Qi, Chuanming Wang, Huiyuan Fu, and Huadong Ma. Coarse-to-fine video denoising with dual-stage spatial-channel transformer. *arXiv preprint arXiv:2205.00214*, 2022.

[88] Syed Waqas Zamir, Aditya Arora, Salman Khan, Munawar Hayat, Fahad Shahbaz Khan, Ming-Hsuan Yang, and Ling Shao. Multi-stage progressive image restoration. In *IEEE Conference on Computer Vision and Pattern Recognition*, pages 14821–14831, 2021.

[89] Hongguang Zhang, Yuchao Dai, Hongdong Li, and Piotr Koniusz. Deep stacked hierarchical multi-patch network for image deblurring. In *IEEE Conference on Computer Vision and Pattern Recognition*, pages 5978–5986, 2019.

[90] Kai Zhang, Yawei Li, Jingyun Liang, Jiezhang Cao, Yulun Zhang, Hao Tang, Radu Timofte, and Luc Van Gool. Practical blind denoising via swin-conv-unet and data synthesis. *arXiv preprint arXiv:2203.13278*, 2022.

[91] Kai Zhang, Jingyun Liang, Luc Van Gool, and Radu Timofte. Designing a practical degradation model for deep blind image super-resolution. In *IEEE Conference on International Conference on Computer Vision*, 2021.

[92] Kai Zhang, Wangmeng Zuo, Yunjin Chen, Deyu Meng, and Lei Zhang. Beyond a gaussian denoiser: Residual learning of deep cnn for image denoising. *IEEE Transactions on Image Processing*, 26(7):3142–3155, 2017.

[93] Kai Zhang, Wangmeng Zuo, and Lei Zhang. Learning a single convolutional super-resolution network for multiple degradations. In *IEEE Conference on Computer Vision and Pattern Recognition*, pages 3262–3271, 2018.

[94] Yulun Zhang, Kunpeng Li, Kai Li, Lichen Wang, Bineng Zhong, and Yun Fu. Image super-resolution using very deep residual channel attention networks. In *European Conference on Computer Vision*, pages 286–301, 2018.

[95] Yinjie Zhang, Yuanxing Zhang, Yi Wu, Yu Tao, Kaigui Bian, Pan Zhou, Lingyang Song, and Hu Tuo. Improving quality of experience by adaptive video streaming with super-resolution. In *IEEE Conference on Computer Communications*, pages 1957–1966, 2020.

[96] Zhihang Zhong, Ye Gao, Yinqiang Zheng, and Bo Zheng. Efficient spatio-temporal recurrent neural network for video deblurring. In *European Conference on Computer Vision*, pages 191–207, 2020.

[97] Shangchen Zhou, Jiawei Zhang, Jinshan Pan, Haozhe Xie, Wangmeng Zuo, and Jimmy Ren. Spatio-temporal filter adaptive network for video deblurring. In *IEEE International Conference on Computer Vision*, pages 2482–2491, 2019.

[98] Xizhou Zhu, Han Hu, Stephen Lin, and Jifeng Dai. Deformable convnets v2: More deformable, better results. In *Proceedings of the IEEE Conference on Computer Vision and Pattern Recognition*, pages 9308–9316, 2019.

[99] Xizhou Zhu, Weijie Su, Lewei Lu, Bin Li, Xiaogang Wang, and Jifeng Dai. Deformable detr: Deformable transformers for end-to-end object detection. *arXiv preprint arXiv:2010.04159*, 2020.